Benchmarking mean-field approximations to level densities

Y. Alhassid, G. F. Bertsch, C. N. Gilbreth, and H. Nakada

Benchmarking mean-field approximations to level densities

Y. Alhassid,[1], G.F. Bertsch[2], C.N. Gilbreth[1], and H. Nakada[3]

[1] *Center for Theoretical Physics, Sloane Physics Laboratory,*
Yale University, New Haven, Connecticut 06520, USA
[2] *Department of Physics and Institute for Nuclear Theory, Box 351560*
University of Washington, Seattle, Washington 98915, USA
[3] *Department of Physics, Graduate School of Science,Chiba University, Inage, Chiba 263-8522, Japan*

We assess the accuracy of finite-temperature mean-field theory using as a standard the Hamiltonian and model space of the shell model Monte Carlo calculations. Two examples are considered: the nucleus ^{162}Dy, representing a heavy deformed nucleus, and ^{148}Sm, representing a nearby heavy spherical nucleus with strong pairing correlations. The errors inherent in the finite-temperature Hartree-Fock and Hartree-Fock-Bogoliubov approximations are analyzed by comparing the entropies of the grand canonical and canonical ensembles, as well as the level density at the neutron resonance threshold, with shell model Monte Carlo (SMMC) calculations, which are accurate up to well-controlled statistical errors. The main weak points in the mean-field treatments are seen to be: (i) the extraction of number-projected densities from the grand canonical ensembles, and (ii) the symmetry breaking by deformation or by the pairing condensate. In the absence of a pairing condensate, we confirm that the usual saddle-point approximation to extract the number-projected densities is not a significant source of error compared to other errors inherent to the mean-field theory. We also present an alternative formulation of the saddle-point approximation that makes direct use of an approximate particle-number projection and avoids computing the usual three-dimensional Jacobian of the saddle-point integration. We find that the pairing condensate is less amenable to approximate particle-number projection methods due to the explicit violation of particle-number conservation in the pairing condensate. Nevertheless, the Hartree-Fock-Bogoliubov theory is accurate to less than one unit of entropy for ^{148}Sm at the neutron threshold energy, which is above the pairing phase transition. This result provides support for the commonly used "back-shift" approximation, treating pairing as only affecting the excitation energy scale. When the ground state is strongly deformed, the Hartree-Fock entropy is significantly lower than the SMMC entropy at low temperatures due to the missing contribution of rotational degrees of freedom. However, treating the rotational bands in a simple model, we find that the entropy at moderate excitation energies is reproduced to within two units, corresponding to an error in the level density of less than an order of magnitude. We conclude with a discussion of methods that have been advocated as beyond the mean field approximation, and their prospects to ameliorate the issues we have identified.

I. INTRODUCTION

Nuclear level densities are important input in the theory of low-energy nuclear reactions. In situations where the reactions cannot be studied in the laboratory, the need for a reliable theory is evident. Many treatments of the level density of heavy nuclei start from a mean-field theory in Hartree-Fock (HF) or the Hartree-Fock-Bogoliubov (HFB) approximation [1–4]. We mention in particular the work by Hilaire and Goriely [2] which presents results of a comprehensive survey based on the HFB approximation.

While the HF and HFB [5, 6] mean-field approximations have been widely applied and taken as a starting point for more sophisticated theories [7, 8], their inherent accuracy has not been well studied. Our goal in this article is to assess these mean-field approximations by taking the Hamiltonian as known and testing them against a theory that is accurate up to well-controlled statistical errors. The auxiliary-field Monte Carlo method, known as the shell model Monte Carlo (SMMC) in nuclear physics [9, 10], fulfills this role. Given the Hamiltonian and a model space, the only inaccuracy is a controllable statistical error associated with the Monte Carlo sampling. As a finite-temperature method, SMMC is particularly suitable for the calculation of level densities [11, 12].

The SMMC starts from a Hamiltonian that is somewhat restricted but which reproduces all the long-range correlations in a realistic way. These include deformations, pairing gaps and low-energy collective excitations. It is thus well-suited to provide a benchmark for testing the validity of the mean-field treatments of nuclear thermal and statistical properties. We note that the SMMC applies to all nuclei irrespective of whether they are deformed or spherical and independently of the existence of a mean-field pairing condensate. In contrast, the formulas for level densities in HF and HFB depend on the character of the mean-field solution.

In Sec. II we summarize the statistical and thermodynamic tools we will use for the analysis and comparisons. In Sec. III we present in some detail the results of the SMMC calculations for two nuclei, namely ^{148}Sm and ^{162}Dy. The first is a spherical nucleus having a strong pairing condensate in HFB. The second is a well-deformed nucleus with a weak pairing condensate; here the HF is an appropriate mean-field approximation. In Sec. IV we present the HF approximation and its results

for ^{162}Dy, while in Sec. V we discuss the HFB approximation and its results for ^{148}Sm. In Sec. VI we summarize our findings regarding the accuracy of the HF and HFB approximations with some remarks on prospects for extending the mean-field approach to level densities. Finally, the data files from the SMMC, HF and HFB calculations together with the codes to apply them are provided in the Supplementary Material depository accompanying this article.

II. TOOLS OF STATISTICAL THEORY

A. The canonical entropy

A good meeting point for comparing different statistical theories is the canonical entropy function $S_c(\beta, N_p, N_n)$, i.e., the entropy of the canonical ensemble of states having fixed numbers of protons and neutrons N_p, N_n and at inverse temperature β. In the SMMC, the quantity that is most directly computed is the thermal energy $E_c(\beta)$ of the canonical ensemble. The entropy can then computed by integrating the thermodynamic relation

$$dS_c = \beta \, dE_c \qquad (1)$$

as

$$S_c(\beta) = S_c(0) - \int_{E_c(\beta)}^{E_c(0)} \beta' \, dE_c . \qquad (2)$$

This allows one to calculate the partition function Z_c from $Z_c = \exp(-\beta E_c + S_c)$. Alternatively, Z_c can be calculated directly from E_c by integrating the relation

$$d\ln Z_c = -E_c d\beta , \qquad (3)$$

and the canonical entropy is then calculated from $S_c = \ln Z_c + \beta E_c$. Finally, the density of states $\rho(E, N_p, N_n)$ at given energy E and particle numbers N_p, N_n is obtained from Z_c by an inverse Laplace transform, carried out in the saddle-point approximation

$$
\begin{aligned}
\rho(E, N_p, N_n) &= \frac{1}{2\pi i} \int_{-i\infty}^{i\infty} d\beta' \, e^{\beta' E} Z_c \\
&\approx \left(2\pi \left| \frac{\partial E}{\partial \beta} \right| \right)^{-1/2} e^{S_c(\beta)} , \qquad (4)
\end{aligned}
$$

where β in the above expression is determined as a function of E from the saddle-point condition

$$E = -\frac{\partial \ln Z_c}{\partial \beta} = E_c(\beta) . \qquad (5)$$

The entropy of a system whose Hamiltonian is defined in a finite-dimensional model space satisfies a sum rule obtained from (2) in the limit $\beta \to \infty$

$$\int_{E(\beta=\infty)}^{E(\beta=0)} \beta \, dE = S(0) - S(\infty). \qquad (6)$$

For a finite-dimensional model space, the entropy at both end points $\beta = 0$ and $\beta = \infty$ is finite and can be determined analytically. In particular, for even-even nuclei, the entropy at zero temperature $S_c(\infty)$ must be zero.

In the configuration-interaction (CI) shell model, we have a certain number N_p, N_n of nucleons in single-particle model spaces of dimensions D_p, D_n giving a canonical entropy at $\beta = 0$ of

$$S_c(0) = S_p(0) + S_n(0) = \ln \binom{D_p}{N_p} + \ln \binom{D_n}{N_n}. \qquad (7)$$

We have found the sum rule in Eq. (6) useful for testing the computer codes we have employed in this study, and also for setting end points on the entropy plots we show later.

B. The grand canonical entropy

The finite-temperature HF (FTHF) and finite-temperature HFB (FTHFB) approximations are defined in the framework of the grand canonical ensemble which depends on the additional independent variables α_i ($i = p, n$), related to the chemical potentials μ_i by $\mu_i = \alpha_i/\beta$.

The grand canonical entropy S_{gc}, when expressed as a function of the energy E_{gc} and the average number of particles $N_{i,gc}$ of type i in the grand canonical ensemble, satisfies

$$dS_{gc} = \beta dE_{gc} - \sum_{i=p,n} \alpha_i dN_{i,gc} , \qquad (8)$$

and can be calculated as in Eq. (2) for fixed $N_{p,gc}, N_{n,gc}$, i.e., when the grand canonical energy E_{gc} is expressed as a function of β and the given particle numbers $N_{i,gc}$.

The grand canonical entropy at $\beta = 0$ is also a simple function of the dimension of the single-particle shell-model space in the CI shell model, since all correlations disappear in that limit. Choosing values for $\alpha_p = \beta\mu_p, \alpha_n = \beta\mu_n$ (where μ_p, μ_n are chemical potentials) to produce average particle numbers N_p, N_n, we have

$$S_{gc}(0, N_p, N_n) = -\sum_{i=p,n} D_i \left[f_i \ln f_i + (1 - f_i) \ln(1 - f_i) \right] , \qquad (9)$$

where $f_i = N_i/D_i$ are occupation factors for $i = p, n$.

The grand canonical partition $Z_{gc} = Z_{gc}(\beta, \alpha_p, \alpha_n)$ satisfies

$$d\ln Z_{gc} = -E_{gc}d\beta + \sum_i N_{i,gc}d\alpha_i . \qquad (10)$$

The Legendre transform of $\ln Z_{gc}$ with respect to α_i is a function of β and $N_{i,gc}$ defined by $\ln \tilde{Z}_{gc} = \ln Z_{gc} - \sum_i \alpha_i N_{i,gc}$ and satisfies

$$d\ln \tilde{Z}_{gc} = -E_{gc}d\beta - \sum_i \alpha_i dN_{i,gc} . \qquad (11)$$

Thus we can alternatively calculate the grand canonical entropy by integrating $-E_{gc}(\beta, N_{i,gc})$ with respect to β at fixed $N_{i,gc}$ to determine $\ln \tilde{Z}_{gc}$ and then find the entropy from $S_{gc}(\beta, N_{i,gc}) = \ln \tilde{Z}_{gc} + \beta E_{gc}$.

The state density $\rho(E, N_p, N_n)$ is related to the partition function $Z_{gc}(\beta, \alpha_p, \alpha_n)$ by the three-dimensional inverse Laplace transform

$$\rho(E, N_p, N_n) = \frac{1}{(2\pi i)^3} \int_{-i\infty}^{i\infty} d\beta \int_{-i\infty}^{i\infty} d\alpha_p \int_{-i\infty}^{i\infty} d\alpha_n \\ \times e^{\beta E - \alpha_p N_p - \alpha_n N_n} Z_{gc}(\beta, \alpha_p, \alpha_n) \quad (12)$$

Normally one carries out the integration over all three variables in the three-dimensional (3-D) saddle-point approximation, resulting in the formula for the state density [13]

$$\rho(E, N_p, N_n) = \frac{1}{(2\pi)^{3/2}} \left| \frac{\partial(E, N_p, N_n)}{\partial(\beta, \alpha_p, \alpha_n)} \right|^{-1/2} e^{S_{gc}}, \quad (13)$$

where the values of $\beta, \alpha_p, \alpha_n$ are determined from E, N_p, N_n by the saddle-point conditions

$$E = -\frac{\partial \ln Z_{gc}}{\partial \beta} = E_{gc}(\beta, \alpha_p, \alpha_n) ,$$
$$N_i = \frac{\partial \ln Z_{gc}}{\partial \alpha_i} = N_{i,gc}(\beta, \alpha_p, \alpha_n) . \quad (14)$$

Using Eqs. (14), the Jacobian in (13) can be written as the determinant of the matrix of second derivatives of the logarithm of the grand canonical partition function with respect to $\beta, \alpha_p, \alpha_n$.

C. Ensemble reduction

To compare the mean-field entropies to the canonical SMMC entropies we need to reduce the grand canonical ensemble of the mean-field formalism to the canonical ensemble. For approximate theories such as the HF and HFB, the only consistent way (in the sense of Appendix II) to carry out the reduction is the variation-after-projection method (VAP), but this is difficult and as far as we know, has never been put into practice for calculating level densities in heavy nuclei. We will therefore only consider simpler reduction methods, recognizing that they cannot be free from ambiguity.

A straightforward way to determine a canonical entropy is to separate the 3-D saddle-point integration Eq. (12) into two steps, integrating first over the chemical variables (α_p, α_n). This yields the following expression for the integrand of the β integration:

$$\zeta^{-1} Z_{gc}(\beta, \alpha_p, \alpha_n) e^{\beta E - \sum_i \alpha_i N_i} , \quad (15)$$

where

$$\zeta = 2\pi \left| \frac{\partial(N_p, N_n)}{\partial(\alpha_p, \alpha_n)} \right|^{1/2} . \quad (16)$$

and α_p, α_n are determined by the 2-D saddle-point conditions $N_i = \partial \ln Z_{gc}/\partial \alpha_i$ $(i = p, n)$. Comparing with the integrand in Eq. (4), we can identify the approximate canonical partition function as

$$\ln Z_c \approx \ln Z_{gc} - \sum_i \alpha_i N_i - \ln \zeta . \quad (17)$$

If we carry out in a second step the β integration of Eq. (15), we obtain an expression of the same form as in Eq. (4) where the approximate canonical entropy is given by

$$S_c \approx S_{gc} - \ln \zeta . \quad (18)$$

The expression we find for the state density ρ is equivalent to Eq. (13) of the 3-D saddle-point approximation [14].

However, the above result does not take into account the variation of the prefactor ζ with respect to β. If we consider this dependence explicitly when we perform the β integration, the saddle-point condition that determines β in terms of the energy E becomes $E = E_\zeta$, where E_ζ is an approximate canonical energy given by

$$E_\zeta = E_{gc} - \delta E, \ \text{ with } \ \delta E = -\frac{d \ln \zeta}{d \beta} . \quad (19)$$

The level density is then given by the canonical form (4), where the canonical entropy is

$$S_c(\beta, N_p, N_n) = S_{gc} - \ln \zeta + \beta \delta E . \quad (20)$$

A simple model is presented in Appendix I, showing that the saddle-point shift δE in Eq. (19) improves the accuracy of the calculated $S_c(\beta)$ and $\rho(E)$.

D. Discrete Gaussian model and the particle-number fluctuation

Another source of error may arise from the Gaussian approximation in the 2-D saddle-point integration used to derive Eq. (16). For example, suppose that the grand canonical partition function were dominant by a single nuclide (N_p, N_n) in some range of α_p, α_n. Then we could approximate $Z_{gc}(\beta, \alpha_p, \alpha_n) \approx Z_c(\beta, N_p, N_n) \exp(\alpha_p N_p + \alpha_n N_n)$. Treating this in the saddle-point Gaussian integration gives $\zeta = 0$ (since N_i are independent of α_j), rather than the correct answer of $\zeta = 1$. The problem can be repaired by recognizing that N_p and N_n are discrete integers, not continuous variables. We calculate the matrix $\partial N_i / \partial \alpha_j$ as before but now we calculate ζ as a discrete sum over particle numbers N_i,

$$\zeta = \sum_{N_i', N_j'} \exp \left(-\frac{1}{2} \sum_{i,j} \frac{\partial N}{\partial \alpha} \Big|_{ij}^{-1} (N_i' - N_i)(N_j' - N_j) \right) . \quad (21)$$

Expression (21) for ζ reduces to the saddle-point result (16) in the limit when the r.h.s. of (16) is large, but has the advantage that it is always larger than 1 and it approaches 1 when the r.h.s. of (16) goes to 0.

To see more physically how the approximation (21) works, consider the case when there is only one type of particles, say neutrons, and the Hamiltonian used in the Gibbs density operator is independent of β and α_i. The required derivative is then

$$\frac{\partial^2 \ln Z_{gc}}{\partial \alpha_n^2} = \frac{\partial N_n}{\partial \alpha_n} = \langle (\Delta N_n)^2 \rangle , \qquad (22)$$

where $\langle (\Delta N_n)^2 \rangle = \langle \hat{N}_n^2 \rangle - N_n^2$ is the neutron-number fluctuation in the grand canonical ensemble. Carrying out the Gaussian saddle-point integration, ζ^{-1} in the 2-D saddle-point approximation (15) becomes

$$\zeta_n^{-1} = \left(2\pi \langle (\Delta N_n)^2 \rangle \right)^{-1/2} . \qquad (23)$$

ζ_n^{-1} is just the ratio of states with particle number N_n to the total number of states in an ensemble in which the particle number N_n' is distributed as a discrete Gaussian

$$P_{N_n'} = \zeta_n^{-1} e^{-(N_n' - N_n)^2 / 2\langle (\Delta N_n)^2 \rangle} \qquad (24)$$

in the limit that $\langle (\Delta N_n)^2 \rangle >> 1$.

The finite-temperature mean-field approximation also provides a many-particle density matrix, so that the particle-number fluctuation can be calculated directly from this density matrix (see Eqs. (37) and (47) below). In fact, this direct calculation is much easier to carry out than calculating numerically the matrix of second derivatives of the logarithm of the partition function. However, because the canonical reduction is not carried out in a variational way, the two methods are not guaranteed to give the same answer. In the sections below, we will examine and compare both methods of carrying out the canonical reduction.

A simplifying approximation that will be examined in Sec. IV below is to assume that the off-diagonal particle-number correlations $\langle \Delta N_i \Delta N_j \rangle$ vanish for $i \neq j$. Then ζ factorizes into two separate factors for protons and neutrons

$$\zeta = \zeta_p \zeta_n, \quad \text{where} \quad \zeta_i = \sum_{N_i'} e^{-(N_i' - N_i)^2 / 2\langle (\Delta N_i)^2 \rangle} . \qquad (25)$$

ζ_i in Eq. (25) can be considered as the partition function which describes the fluctuations in the number of particles of type i. The reduction from the grand canonical to the canonical partition function is then given by

$$Z_{gc}(\beta, \alpha_p, \alpha_n) e^{-\sum_i \alpha_i N_i} \approx Z_c(\beta, N_p, N_n) \zeta_p \zeta_n . \qquad (26)$$

Relation (26) describes the factorization of the grand canonical partition function into a canonical partition function and particle-number fluctuation partition functions. It is exact in the simple model presented in Appendix I.

In summary, the saddle-point approximation breaks down when $2\pi \langle (\Delta N_i)^2 \rangle \leq 1$. However, ζ in the discrete Gaussian model (Eqs. (25) and (26) or Eq. (21)) always satisfies $\zeta \geq 1$ and can be used even when the particle-number fluctuation is small. We will demonstrate the improvement to the saddle-point formula in this limit in the case of ^{162}Dy (Sec. IV B) where pairing correlations are weak.

E. Spin-parity projected level density

The ultimate goal is to calculate the spin-parity projected densities $\rho_{J^\pi}(E)$, defined as the number of levels of given angular momentum J and parity π per unit energy, not counting the $2J + 1$ magnetic degeneracy of the levels. The spin-dependent level densities $\rho_{J^\pi}(E)$ can be calculated through an angular momentum projection. The present paper is mainly focussed on the total state density and we will not examine in details spin-projection methods. However, to make at least a tentative comparison of the level density at the neutron resonance threshold we will calculate them taking a simplified model for the spin-parity projection. We follow common practice and assume the spin distribution is Gaussian in the three components of the angular momentum vector $\vec{J}$ [15]. Then the fraction of levels having angular momentum J is given by

$$P_J \approx \sqrt{\frac{1}{2\pi}} \frac{J + \frac{1}{2}}{\sigma^3} \exp \left(-\frac{(J + \frac{1}{2})^2}{2\sigma^2} \right) . \qquad (27)$$

Here a pre-exponential factor of $(J + \frac{1}{2})^2$, arising from the three-dimensional volume element of $\vec{J}$, is reduced to the first power of $(J + \frac{1}{2})$ by dividing out the $(2J + 1)$ magnetic degeneracy factor. The parameter σ, known as the spin cutoff parameter, is estimated from the second moment of J_z

$$\sigma^2 = \langle J_z^2 \rangle . \qquad (28)$$

The normalization condition of P_J in (27) is $\sum_J (2J + 1) P_J = 1$. Assuming equal positive- and negative-parity level densities (usually justified at the neutron separation energy), we have

$$\rho_{J^\pi}(E) \approx \frac{1}{2} P_J \rho(E) . \qquad (29)$$

III. SMMC RESULTS

The SMMC method is formulated in the framework of a CI spherical shell-model Hamiltonian. The CI Hamiltonians shown to be amenable to Monte-Carlo sampling contain one- plus two-body operators, with the two-body part restricted to interactions that have a "good sign" in the grand canonical formulation [16]. In finite nuclei, the method is implemented with particle-number

projection [17] for both protons and neutrons, and the calculated observables are the expectation values in the canonical density matrix. In particular, we consider here the nuclei ^{148}Sm and ^{162}Dy. The nucleus ^{148}Sm is an example of a heavy spherical nucleus whose ground state has significant correlation energy associated with pairing, while the nucleus ^{162}Dy has a deformed ground state with weak pairing.

The parameterization of the Hamiltonian and other aspects of the SMMC calculation have been published elsewhere [18, 19]. For reference, Table I and its caption describes the model space employed in the calculations.

	N_i	d_i	$S_{c,i}(0)$	$S_{gc,i}(0)$
^{148}Sm n	16	$8.5 \cdot 10^{14}$	34.38	36.55
^{148}Sm p	12	$5.6 \cdot 10^{9}$	22.44	24.43
^{162}Dy n	26	$1.6 \cdot 10^{18}$	41.95	44.25
^{162}Dy p	16	$6.3 \cdot 10^{10}$	24.86	26.92

TABLE I: Model space parameters for the SMMC Hamiltonian in ^{162}Dy and ^{148}Sm and corresponding canonical and grand canonical entropies at $\beta = 0$. The single-particle basis employed in the CI spherical shell model consists of the orbitals $0g_{7/2}, 1d_{5/2}, 1d_{3/2}, 2s_{1/2}, 0h_{11/2}, 1f_{7/2}$ for protons and $0h_{11/2}, 0h_{9/2}, 1f_{7/2}, 1f_{5/2}, 2p_{3/2}, 2p_{1/2}, 0i_{13/2}, 1g_{9/2}$ for neutrons. The numbers of the single-particle states (including their magnetic degeneracy) are $D_p = 40$ and $D_n = 66$. N_i are the number of valence particles of type i (where the index i distinguishes neutrons and protons), and d_i is the dimension of the many-particle model space for particles of type i. The canonical and grand canonical entropies $S_{c,i}(0)$ and $S_{gc,i}(0)$ are calculated from Eqs. (7) and (9), respectively.

The canonical energy $E_c = \langle \hat{H} \rangle_{N_p, N_n}$ and the mean square angular momentum $\langle \hat{J}^2 \rangle_{N_p, N_n}$ at fixed numbers of protons and neutrons are calculated directly in SMMC as a function of β. Table II shows the SMMC energies at $\beta = 0$ (i.e., the infinite temperature limit) and at high β extrapolated to infinity. The energy at $\beta = 0$ is largely determined by the one-body part of the Hamiltonian in the grand canonical ensemble.

The variation of the excitation energy E_x with β is shown in Fig. 1 using a logarithmic scale for the energy. The excitation energy of ^{162}Dy is higher than that of ^{148}Sm from $\beta = 0$ to $\beta \approx 1.5$ and is then lower up to $\beta \approx 3.5$. The higher excitation energy in ^{148}Sm near $\beta = 3$ is likely due to the collapse of strong pairing in that nucleus. Similarly, the higher ^{162}Dy excitation energy at $\beta \approx 1$ may be ascribed to the loss of deformation energy in that temperature region.

We also need the $\langle \hat{J}^2 \rangle$ ensemble averages to calculate the spin-dependent level densities. These are shown in Fig. 2 for ^{148}Sm and ^{162}Dy. The higher values of $\langle \hat{J}^2 \rangle$ of ^{162}Dy at high β are largely due to its deformation and its low-lying first excited 2^+ state at ~ 0.08 MeV. In contrast, $\langle \hat{J}^2 \rangle$ for ^{148}Sm decreases dramatically at high β, as expected for a nucleus with a $J = 0$ ground state and a gap of ~ 0.5 MeV to the first excited $J = 2$ state.

nucleus	β	SMMC	HF	HFB	correlation energy HF/HFB	missing
^{148}Sm	0	-119.15	-119.0	-119.0		
	∞	-235.65 ± 0.015	-230.69	-232.51	1.82	3.14
^{162}Dy	0	-238.35	-238.12	-238.12		
	∞	-375.39 ± 0.02	-371.78	-371.91	11.41	3.48

TABLE II: Limiting values of the energies (MeV) calculated by SMMC, HF, and HFB for ^{148}Sm and ^{162}Dy. The HF/HFB correlation energy is the energy difference between HF and HFB ground states for ^{148}Sm, and the difference between spherical and deformed ground states for ^{162}Dy. The term "missing" denotes the differences between the HFB energies (with both pairing and deformation) and the SMMC ground-state energies. The SMMC energies at $\beta = \infty$ include extrapolation and statistical sampling errors [18].
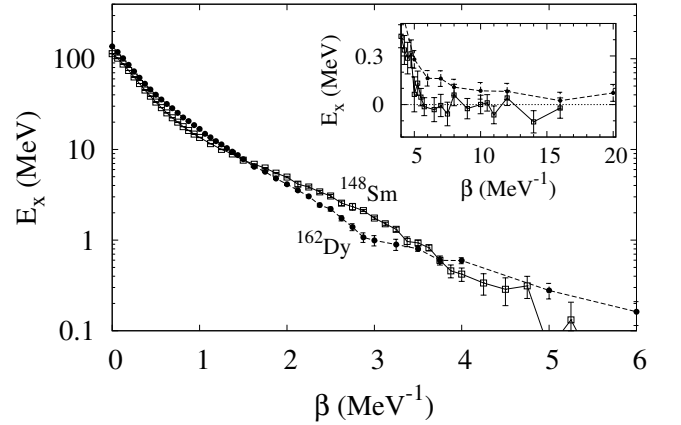

FIG. 1: Canonical excitation energies E_x (on a logarithmic scale) versus β calculated by the SMMC for ^{148}Sm (open squares) and for ^{162}Dy (solid circles), with lines drawn to guide the eye. The inset shows the large β values using a linear scale for the excitation energy. The Monte Carlo statistical errors are about 0.1 MeV or smaller.

At low β, the remaining enhancement for ^{162}Dy is due to its larger number of active valence nucleons in the model space. The errors shown in Fig. 2 are statistical errors from the Monte Carlo sampling.

We next apply Eq. (2) to compute the canonical SMMC entropy. We start from $\beta = 0$ with the initial value of the canonical entropy given by Eq. (7) and use the relation

$$\int_{E_c(\beta)}^{E_c(0)} \beta' dE_c = -\beta E_c(\beta) + \int_0^\beta E_c(\beta') d\beta' , \qquad (30)$$

where $E_c(\beta)$ is the canonical thermal energy calculated in SMMC as the thermal expectation value of the Hamiltonian. The results are shown in Fig. 3, with the main figure showing the low to intermediate values of β, and
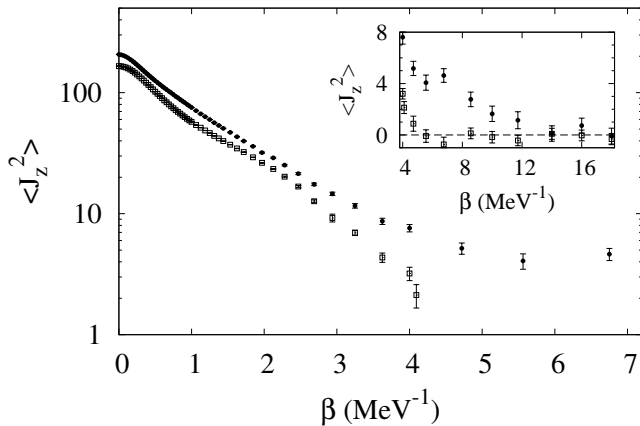
FIG. 2: SMMC values of $\langle J_z^2 \rangle = \langle \vec{J}^2 \rangle / 3$ (shown using a logarithmic scale) vs. β in the canonical ensembles for ^{148}Sm (open squares) and ^{162}Dy (solid circles). The inset shows $\langle J_z^2 \rangle = \langle \vec{J}^2 \rangle / 3$ (using a linear scale) for larger β values.
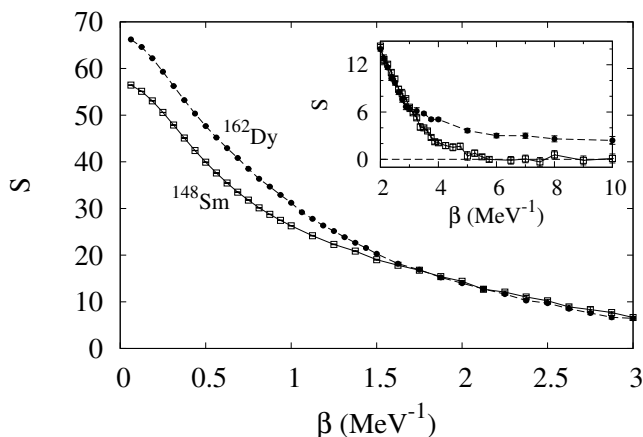

FIG. 3: SMMC entropies of ^{148}Sm (open squares) and ^{162}Dy (solid circles) for $\beta < 3$ MeV^{-1}. In this range, the Monte Carlo errors are the size of the symbols or smaller. The inset shows the entropies for the larger β values.

the inset showing the large values of β.

The ^{148}Sm and ^{162}Dy entropies are nearly equal for β in the range $1.5 - 3.0$ MeV^{-1}. We do not know any obvious reason why that should be the case. At higher values of β, shown in the inset, one observes a difference between the two nuclei. For ^{148}Sm at $\beta \geq 6$ MeV^{-1} the entropy is essentially zero, as expected at low temperatures for even-even nucleus with a pairing gap. On the other hand, the entropy of ^{162}Dy remains a couple of units higher than zero up to at least $\beta \sim 10$ MeV^{-1}. This is due to the low excitations associated with the ground-state rotational band, together with the weak pairing in

this nucleus.

The state densities calculated from Eq. (4) are shown in Fig. 4. As expected, the state density is higher for ^{162}Dy than ^{148}Sm at low excitation energy. Interestingly, they become much closer at excitation energies in the range 5-10 MeV. As a check on the quality of the
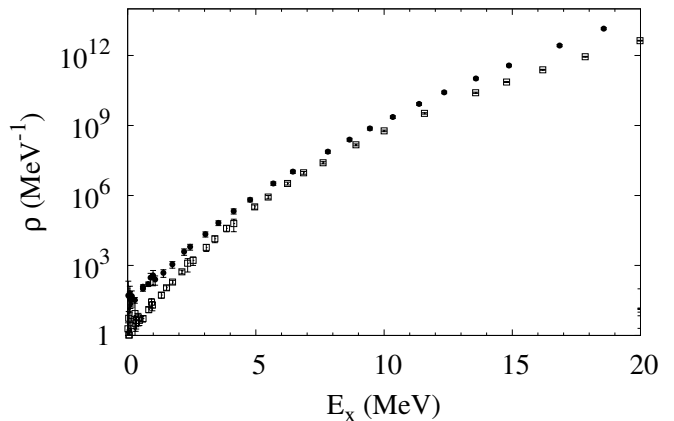

FIG. 4: State densities vs. excitation energy E_x calculated in SMMC using the saddle-point expression Eq. (4) for ^{162}Dy (solid circles) and ^{148}Sm (open squares). The range is truncated at the lower end because the saddle-point approximation breaks down when there are only a few levels in a range β^{-1} around E.

CI Hamiltonian, we compare the calculated level densities with the experimental s-wave resonance spacings $D = [\sum_J \rho_{J^\pi}(E)]^{-1}$, measured at an energy E that corresponds to the neutron separation energy. These are calculated from the spin-parity dependent level density (29) and (27), taking the spin cutoff parameter σ from Eq. (28). The results are shown in Table III. The agreement to within a factor of two or better gives us confidence that the Hamiltonian is realistic enough to provide useful tests of the HF and HFB approximations.

Nucleus	E_x (MeV)	J^π	D (eV)			
			SMMC	HF	HFB	Exp.
^{148}Sm	8.1	$(3^-, 4^-)$	3.7 ± 0.6		4.1	5.7
^{162}Dy	8.2	$(2^+, 3^+)$	2.4 ± 0.3	0.5		2.4

TABLE III: s-wave resonance spacings D at the excitation energy E_x that corresponds to the neutron separation energy. J^π are the values of spin and parity of the relevant neutron resonance levels. The SMMC, HF and HFB results are compared with the experimental values from Ref. 34. The HF spacing is calculated using the model of Sec. IV B 5 to estimate the contribution of rotational bands.

IV. THE FINITE-TEMPERATURE HF APPROXIMATION

The finite-temperature theory is derived from a variational principle based on the grand potential Ω as a function of an uncorrelated trial density [5, 6]. We first consider the HF approximation, where the density is uniquely characterized by a one-body density matrix ϱ_{kl}, where k, l label single-particle orbitals in the model space.

For simplicity, we consider only one type of particles and the results are easily generalized to both protons and neutrons. At the FTHF minimum, the one-body density ϱ satisfies the self-consistent equation

$$\varrho = \frac{1}{e^{\beta h_\varrho - \alpha} + 1} \, , \tag{31}$$

where $h_\rho = t + v\varrho$ is the one-body HF Hamiltonian, expressed respectively in terms of the one- and two-body matrices t and v of the configuration-interaction shell model Hamiltonian. The value of Ω at the HF minimum is given by

$$\beta\Omega_{HF} = -\ln Z_{HF} = \beta E_{HF} - S_{HF} - \alpha N_{HF} \, , \tag{32}$$

where Z_{HF} is the HF approximation to the grand canonical partition function. The thermal HF energy E_{HF} is calculated as

$$E_{HF} = \text{tr}(t\varrho) + \frac{1}{2}\text{tr}(\varrho v \varrho) \, , \tag{33}$$

the entropy S_{HF} is given by

$$\begin{aligned} S_{HF} &= -\text{tr}(\varrho \ln \varrho) - \text{tr}[(1-\varrho)\ln(1-\varrho)] \\ &= -\sum_k f_k \ln f_k - \sum_k (1-f_k)\ln(1-f_k) \, , \end{aligned} \tag{34}$$

and the average number of particles N_{HF} is computed as

$$N_{HF} = \text{tr}\,\varrho \, . \tag{35}$$

The occupation probabilities $f_k = [1 + e^{\beta(\epsilon_k - \mu)}]^{-1}$ are the usual Fermi-Dirac occupations where ϵ_k are the single-particle HF energies at inverse temperature β.

It is not obvious from Eqs. (32), (33) and (35) that $\ln Z_{HF}$ satisfies the thermodynamic derivative relations (14) due to the dependence of the HF single-particle energies and density on α and β. Nevertheless, the contributions to the derivatives that originate in the implicit dependences on α and β vanish. In particular, the quantities defined in the HF theory satisfy

$$-\frac{\partial \ln Z_{HF}}{\partial \beta} = E_{HF} \, , \quad \frac{\partial \ln Z_{HF}}{\partial \alpha_i} = N_{i,HF} \, . \tag{36}$$

The proof is provided in Appendix II. The validity of these relations in FTHF guarantee that the grand canonical HF entropy S_{HF} satisfies the relation $dS_{HF} = \beta dE_{HF}$ at fixed average particle numbers $N_{i,HF} = N_i$, and thus we can compute the entropy in the same way as we did in the SMMC.

A. Approximate canonical projectors in FTHF

The canonical partition function can be approximated either in the saddle-point approximation of Sect. II C or in the discrete Gaussian model of Sect. II D. However, the connection to particle-number fluctuations is more tenuous because the second derivative expressions for $\ln Z_{gc}$ in terms of particle-number fluctuations such as Eq. (22) no longer holds for $\ln Z_{HF}$. Nevertheless, it is interesting to compare ζ computed with the full matrix $\partial N_i/\partial \alpha_j$ to that computed from the particle-number fluctuations. We make such a comparison for ^{162}Dy in the next section.

B. Application to ^{162}Dy

Here we discuss the strongly deformed nucleus ^{162}Dy. The pairing in this nucleus is weak, so that the FTHF is the appropriate mean-field theory.

1. Number partition function ζ

We first examine the number partition function ζ obtained from the approximations we presented in Sec. II. The diagonal particle-number fluctuations in FTHF are given by

$$\langle (\Delta \hat{N}_i)^2 \rangle = \text{tr}[\varrho_i(1-\varrho_i)] \tag{37}$$

and the off-diagonal ones are zero. The corresponding ζ obtained from Eq. (25) is shown as the dashed line in Fig. 5. This is compared to ζ calculated from Eq. (21) (using the matrix $\partial N_i/\partial \alpha_j$), shown as the solid line. They differ by less than 10%, except for a tiny region near the spherical-to-deformed phase transition. There the ζ calculated from the Jacobian of $\partial N_i/\partial \alpha_j$ diverges (when approached from the deformed side). Thus, it appears to be a very good approximation to calculate ζ in term of the individual particle-number fluctuations as in Eq. (25). In the next section, we shall see that this is not the case for the FTHFB theory in the presence of strong pairing correlations. In any case, we will use Eq. (21) in the results shown below.

2. Thermal excitation energy

The range of FTHF energies as a function of β is shown in the fourth column of Table II. The high-temperature limit is very close to the SMMC value, since all correlation energies disappear in that limit. At the other limit of large β, at or near the ground state, the SMMC energy is about 3.5 MeV lower than its HF value. The HF ground-state energy has the correlations associated with the static deformation, but is missing the rotational energy and other correlation effects. It can also be seen
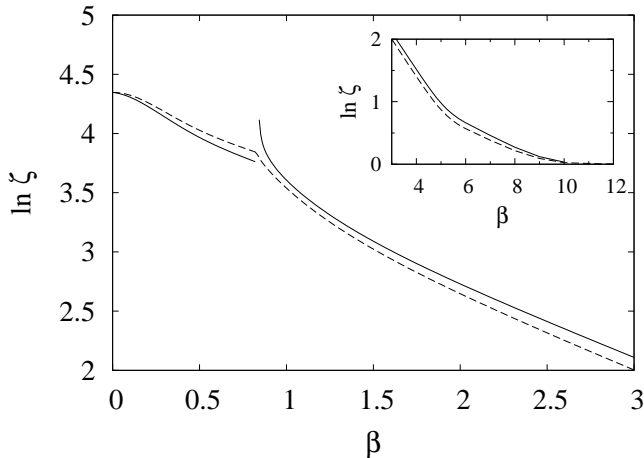
FIG. 5: $\ln\zeta$ vs. β in FTHF for ^{162}Dy. Solid line: $\ln\zeta$ calculated from Eq. (21). Dashed line: $\ln\zeta$ calculated from Eq. (25).

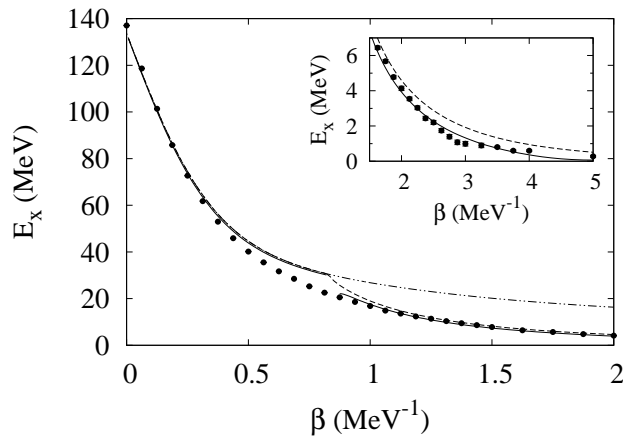from the fifth column of Table II that the HFB approximation hardly lowers the energy. The excitation energy

FIG. 6: The HF excitation energy of ^{162}Dy vs. β. The grand canonical HF energy (dashed line) is compared with the approximate canonical energy E_ζ (solid line) from Eq. (19). The latter omits the region near the shape transition point, where ζ becomes singular (see solid line in Fig. 5). We also show the energy for the spherical HF solution (dashed-double dotted line) with respect to the deformed ground-state energy. The solid circles are the SMMC excitation energies from Fig. 1. Inset: expanded energy scale for higher β values.

$E_x(\beta)$ is shown in Fig. 6, comparing its HF value (solid line) with the SMMC thermal energy (solid circles) from Fig. 1. The HF density is spherical for $\beta < 0.9$ and becomes deformed above that value. The energy of the spherical HF solution at higher values of β is shown in Fig. 6 by the dashed-double dotted line. We observe

that the HF energy has a cusp at the onset of deformation. Extrapolating the energy of the spherical solution to large β, we find that the deformed ground-state solution is lower in energy than the spherical solution by 11.4 MeV. The SMMC energy, shown by the solid circles, is remarkably close to the HF energy in the region $0 < \beta < 3$ MeV^{-1} except in the vicinity of the shape phase transition. The cusp in the HF energy function disappears in the SMMC energy, leaving no trace of a shape phase transition. The fact that mean-field theory over-emphasizes phase transitions in finite systems is well-known in nuclear theory; see, e.g., in Refs. 1, 20–22. The inset in Fig. 6 shows $E_x(\beta)$ at higher values of β using a finer energy scale. We observe that at large β the grand canonical HF energy (dashed line) overestimates the excitation energy but that the approximate canonical energy E_ζ of Eq. (19) (solid line) is in overall good agreement with the SMMC excitation energy.

3. Entropies

The grand canonical HF entropy S_{HF} is shown in Fig. 7 as a function of β (dashed line) and compared with the approximate canonical entropy (20) with ζ from the discrete Gaussian formula Eq. (21) (solid line). At $\beta = 0$, the grand canonical HF entropy is larger than the canonical entropy due to particle-number fluctuations. The entropies at large values of β are shown in the inset. The grand canonical HF entropy vanishes in the limit $\beta \to \infty$, as expected. However, the saddle-point canonical entropy calculated from Eqs. (15) and (16) increases at large values of β (dotted line in the inset), indicating the breakdown of the saddle-point approximation to the particle-number projection. In contrast, the discrete Gaussian treatment (21) gives an entropy that approaches zero at high β, thus satisfying the sum rule Eq. (6). For moderate and small values of β, the entropy (20) of the discrete Gaussian model (21) essentially coincides with the saddle-point canonical entropy. As noted earlier, the SMMC entropy remains nonzero in the range $8 < \beta < 15$. We examine this further in the next paragraph.

To compare the projected HF and SMMC entropies in more detail, we have replotted them in Fig. 8 with some additional information. Both curves start at the same value at $\beta = 0$ because the model spaces are identical. In the limit of large β, the SMMC entropy does not approach zero as fast as the canonical HF entropy. This is because the SMMC entropy includes a contribution from the ground-state rotational band, most visible at $\beta > 5$ MeV^{-1}. We can estimate this contribution as follows. The moment of inertia $\mathcal{I}_{gs}$ of the ground-state band of ^{162}Dy was determined to be $\mathcal{I}_{gs}/\hbar^2 = 35.8 \pm 1.5$ MeV^{-1} by fitting the low-temperature SMMC values of $\langle \vec{J}^2 \rangle$ to $\langle \vec{J}^2 \rangle = 2(\mathcal{I}_{gs}/\hbar^2)T$ [18]. For $\beta < 20$ MeV^{-1}, $T > \hbar^2/2\mathcal{I}_{gs}$, and we can treat the rotational motion classically. The classical partition function of the rotational
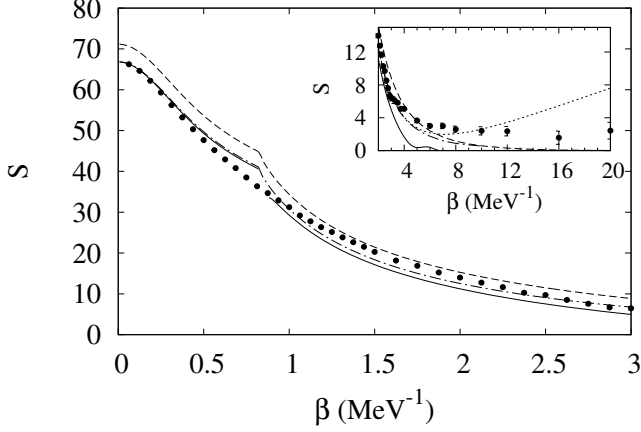
FIG. 7: Entropy of ^{162}Dy in the FTHF approximation, comparing the grand canonical entropy (dashed line) with the canonical entropy defined in Eqs. (20) and (19) (solid line). The dashed-dotted line is the approximate canonical entropy (18) in the 3-D saddle-point approximation, i.e., without the correction term in Eq. (19). The inset shows the large β value. The calculations use the discrete Gaussian model formula (21) for ζ. The dotted line in the inset uses the saddle-point expression Eq. (16) for $\beta > 5$ MeV^{-1}.
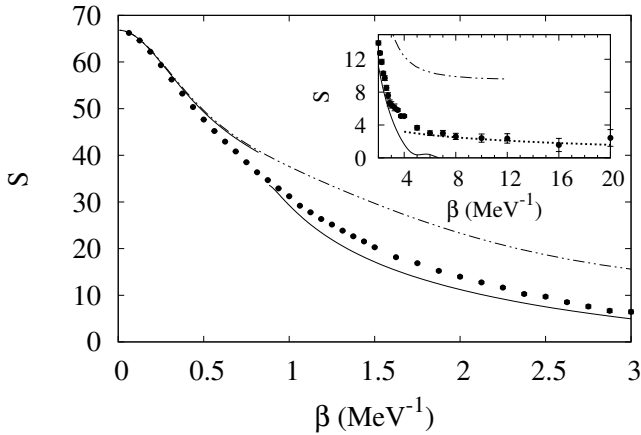
FIG. 8: Approximate canonical HF entropy defined by Eqs. (20) and (19) for ^{162}Dy (solid line) is compared with the SMMC entropy (solid circles). The dashed-double dotted line is the canonical entropy of the spherical HF solution in the same approximation. The inset shows the entropies at large values of β. The dotted line in the inset is the ground-state rotational band contribution (38).

band $J = 0, 2, \ldots$ is given by $Z_{rot} = \mathcal{I}_{gs}T/\hbar^2$. We can then calculate its entropy from $S_{rot} = -\partial F_{rot}/\partial T$, where $F_{rot} = -T \ln Z_{rot}$ is the free energy of the ground-state

rotational band. We find

$$S_{rot} = 1 + \ln\left(\frac{\mathcal{I}_{gs}}{\hbar^2}T\right) . \qquad (38)$$

This contribution is described by the dotted line in the inset of Fig. 8, and is in good agreement with the SMMC entropy at large β with no adjustable parameters.

We also show in Fig. 8 the canonical entropy of the spherical HF solution (dashed-double dotted line). This entropy approaches a finite non-zero value in the limit $\beta \to \infty$ (see inset) because of the large degeneracy of the spherical HF solutions at $T = 0$. There are 2 valence protons in the $0h_{11/2}$ orbitals and 6 valence neutrons in the $0h_{9/2}$ orbitals, leading to a highly degenerate ground state with a canonical entropy of $\ln\left[\binom{12}{2}\binom{10}{6}\right] = 9.54$. The grand canonical HF entropy in this limit is even larger. It can be calculated assuming the uniform filling of the valence degenerate orbitals in the $T \to 0$ limit of the HF approximation. The corresponding formula has the form of Eq. (9), where $D_p = 12$, $f_p = 2/12$ and $D_n = 10$, $f_n = 6/10$ and gives a grand canonical entropy of 13.33.

4. Angular momentum fluctuations

In HF, the variance of the angular momentum components J_q ($q = x, y, z$) can be calculated using Wick's theorem as

$$\langle(\Delta J_q)^2\rangle = \langle \hat{J}_q^2\rangle - \langle \hat{J}_q\rangle^2 = \text{tr}[j_q\,(1-\varrho)j_q\,\varrho] , \qquad (39)$$

where j_q is the matrix representing $\hat{J}_q$ in the single-particle space. When the HF equilibrium ensemble is axially symmetric around the z-axis, ϱ is invariant under rotations around the z axis and $\langle \hat{J}_x\rangle = \langle \hat{J}_y\rangle = 0$. Assuming time-reversal invariance, we also have $\langle \hat{J}_z\rangle = 0$. It follows that the variances of the angular momentum components are the same as the mean square moments. In Fig. 9, we compare the HF mean square moments of $\hat{J}_x$ and $\hat{J}_z$ (solid lines) with the SMMC moments $\langle \hat{J}_x^2\rangle = \langle \hat{J}_y^2\rangle = \langle \hat{J}_z^2\rangle = \langle \hat{J}^2\rangle/3$ (solid circles) in ^{162}Dy . The HF mean square moments of $\hat{J}_x$ and $\hat{J}_z$ coincide above the shape transition temperature, where the HF solution is spherical. However, at large values β, the HF mean square moment of $\hat{J}_x$ is much larger than the respective moment of $\hat{J}_z$. Since the deformed intrinsic ground state has good $K = 0$, $\langle \hat{J}_z^2\rangle$ approaches zero in the limit $\beta \to \infty$, while $\langle \hat{J}_x^2\rangle$ remains finite and large in this limit. We also show by dashed line $\langle \hat{J}_x^2\rangle$ for the spherical HF solution.

5. State density and level spacing

In Fig. 10 we show the HF density vs. E_x in the saddle-point approximation (4) (solid line) (where the approx-
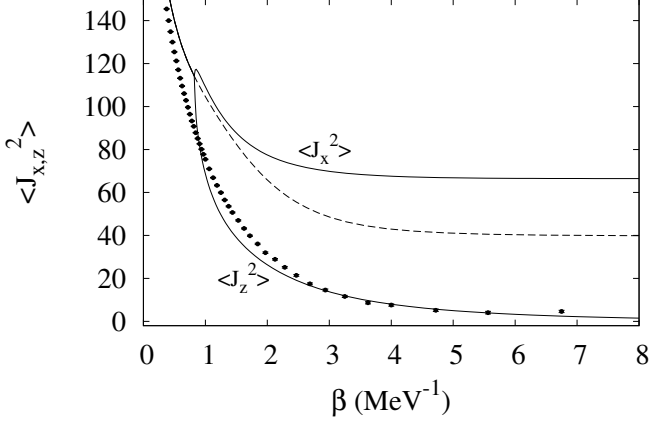
FIG. 9: Second moments of the angular momentum in ^{162}Dy. The solid lines are the HF results which exhibit a kink at the shape transition point. The dashed line describes the spherical HF solution for temperatures where the lowest equilibrium solution is deformed. These HF moments may be compared with the SMMC moments shown by solid circles. The SMMC moments satisfy $\langle J_{x,y}^2 \rangle = \langle J_z^2 \rangle = \langle \vec{J}^2 \rangle / 3$.
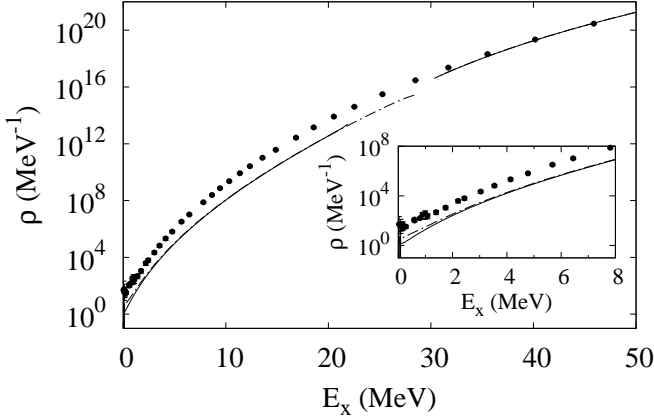

FIG. 10: The HF density of ^{162}Dy calculated in the saddle-point approximation (4) using Eqs. (19) and (20) for the approximate energy and canonical entropy (solid line) is compared with the SMMC state density (solid circles) as a function of excitation energy E_x. The gap in excitation energy reflects the discontinuity of the energy at the shape transition as is seen in Fig. 6. The dashed-dotted line is the approximation in which the δE correction is neglected in the saddle-point energy Eq. (19) and in the approximate canonical entropy of Eq. (20). The inset shows an expanded scale at low excitation energies.

imate canonical entropy and energy include the δE correction in Eqs. (20) and (19) respectively), and compare it with the SMMC state density (solid circles). The kink

in the HF density at $E_x \approx 31$ MeV signifies the shape transition from a deformed to spherical shape. At lower excitation energies, the HF state density underestimates the SMMC values; the SMMC density includes a contribution from rotational bands that are built on top of intrinsic K states, and are not captured in the HF approximation. Above the shape transition energy, the equilibrium shape is spherical and no longer supports rotational bands. The HF density is then very close to the SMMC density.

We can try to repair the HF approximation by recognizing that the each of the deformed HF configurations represents a band [23]. The angular momentum J_z corresponds to the K-quantum number of the band. Assuming that K is Gaussian distributed, the K-dependent HF state density ρ_K can be expressed

$$\rho_K(E) = P_K \rho_{HF}(E). \tag{40}$$

where

$$P_K = \frac{1}{(2\pi\sigma^2)^{1/2}} \exp\left(-\frac{K^2}{2\sigma^2}\right). \tag{41}$$

and

$$\sigma^2 = \langle J_z^2 \rangle. \tag{42}$$

For each positive K there will be a rotational band with $J = K, K+1, ...$ For $K = 0$ the sequence may skip odd or even J values. For a complete treatment of the band model one next introduces a moment of inertia of the band to calculate the J-dependent level density. However, we do not wish to introduce new parameters that take us beyond the HF theory so we assume that all the levels in a band are degenerate. The level density is then

$$\rho_{J^\pi}(E) \approx \frac{1}{2} \sum_{K=0}^{J} \rho_K(E), \tag{43}$$

treating the $K = 0$ bands the same as the others. The factor of $1/2$ is for parity projection. The resulting average resonance spacing at the neutron threshold of $E = 8.2$ MeV for ^{162}Dy is reported in Table III. It underestimates the SMMC value by a factor of ~ 5. This is a substantial disagreement; in our view uncovers a serious problem with the HF theory of level densities in deformed nuclei.

6. Frozen-potential model

An approximation adopted in a number of previous works is to take the HF or HFB ground-state mean fields, and assume the excited states can be calculated with a single-particle potential based on that field. For example, this is done in what is called HF-BCS or HFB approximations in Refs. [1, 2, 4], and in the combinatorial level-density model presented in Ref. [24]. Since

the potential field does not depend on the presence of particle excitations, we will call them frozen-potential (FP) models. For an axially deformed nucleus such as ^{162}Dy, the single-particle HF levels come in doubly degenerate time-reversed pairs and for an even number of particles the ground state is non-degenerate, so that the $T = 0$ entropy is zero. It is rather easy to carry out the exact particle-number projection in the HF FP approximation [25], so we will use it in the comparison. In
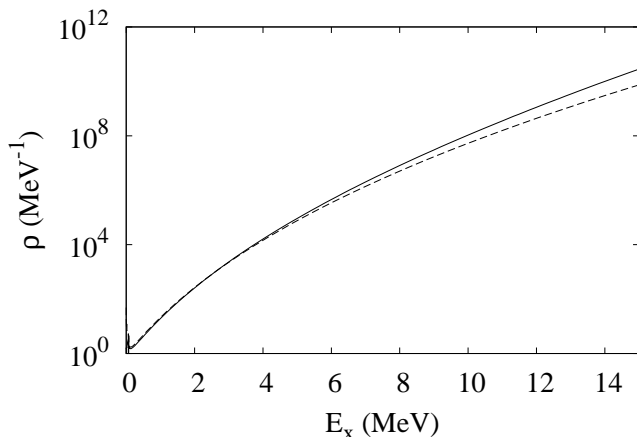
FIG. 11: The particle-projected FP density of ^{162}Dy (dashed line) based on the zero temperature HF single-particle levels is compared with the HF density (solid line from Fig. 10) as a function of excitation energy E_x.

Fig. 11, we compare the FP state density with the FTHF density determined by using Eq. (20) for S_c. They agree very well at low excitation energy. At the neutron separation energy, $S_n \approx 8.2$ MeV, the FP state density is lower than the FTHF density by less than a factor of 2. However, the discrepancy increases with excitation energy, exceeding one unit entropy beyond 15 MeV excitation energy. At the shape phase transition, the FP approximation underestimates the HF density by more than two orders of magnitude. We conclude that FP model is a good approximation at excitation energies that are small compared to the shape transition energy, but not near and above this transition energy.

V. THE FINITE-TEMPERATURE HFB APPROXIMATION

The HFB is the preferred mean-field approximation for nuclei exhibiting strong pairing correlations. Like the FTHF, the FTHFB is based on the grand canonical ensemble. However, unlike the FTHF, the simple approximate particle-number projection onto a canonical ensemble is not expected to be a good approximation at low temperatures. This will be evident as we go through the steps to calculate the level density of ^{148}Sm, starting from

the HFB energy function $E_{HFB}(\beta)$. To simplify the notation, we consider only one type of particles as we did in the FTHF. The HFB thermal energy is expressed in terms of the normal and anomalous densities ϱ, κ as

$$E_{HFB} = \text{tr}(t\varrho) + \frac{1}{2}\text{tr}(\varrho v \varrho) + \frac{1}{4}\text{tr}(\kappa^\dagger v \kappa) . \qquad (44)$$

The HFB entropy $S_{HFB}(\beta)$ is given by

$$S_{HFB} = -\sum_k f_k \ln f_k - \sum_k (1 - f_k) \ln(1 - f_k) , \quad (45)$$

where

$$f_k = \frac{1}{1 + e^{\beta E_k}} \qquad (46)$$

are the quasi-particle occupations expressed in terms of the quasi-particle energies E_k.

The HFB partition function satisfies relations similar to Eqs. (36), and thus the entropy can be computed from the energy function by an integral similar to Eq. (2). All the expressions regarding the level density in Sec. IV carry over to the HFB approximation, except that the particle-number variance in Eq. (37) is now calculated using all three Wick contraction terms in the expectation value $\langle a_k^\dagger a_k a_l^\dagger a_l \rangle$. This leads to an additional contribution from the anomalous density κ

$$\langle (\Delta \hat{N})^2 \rangle = \sum_k \varrho_{kk} - \sum_{kl} |\varrho_{kl}|^2 + \sum_{kl} |\kappa_{kl}|^2 . \qquad (47)$$

A. Application to ^{148}Sm

The mean-field ground state of ^{148}Sm is spherical and has a substantial pairing condensate. Thus FTHFB is the proper mean-field theory for this nucleus. The pairing correlation energy, defined as the difference between the HF and HFB ground-state energies is 1.82 MeV (see Table II). Also shown in Table II is the correlation energy of the SMMC ground state with respect to the HFB solution (i.e., the difference between the HFB and SMMC ground-state energies). This correlation energy is labeled "missing" in the table and is about 3 MeV for ^{148}Sm. The pairing transitions for protons and neutrons occur at $\beta = 2.1$ MeV^{-1} ($E_x = 5.9$ MeV) and $\beta = 2.7$ MeV^{-1} ($E_x = 3.4$ MeV), respectively.

We first examine ζ, the factor used to convert the grand canonical quantities to canonical in the HFB. Naively, we may try using the HFB particle-number fluctuation in Eq. (47) in Eq. (25). The resulting ζ is shown as the dashed line in Fig. 12. This approximation is bound to fail at low temperatures because the mixed particle number in the HFB ground state. We have also calculated ζ from Eq. (21) using the full $\partial N_i / \partial \alpha_j$ matrix suggested by the 3-D saddle-point approximation. This gives a better result for $\beta > 2$ MeV^{-1}, as may be seen by the solid line in Fig. 12. We will therefore use this method for the canonical quantities calculated below.
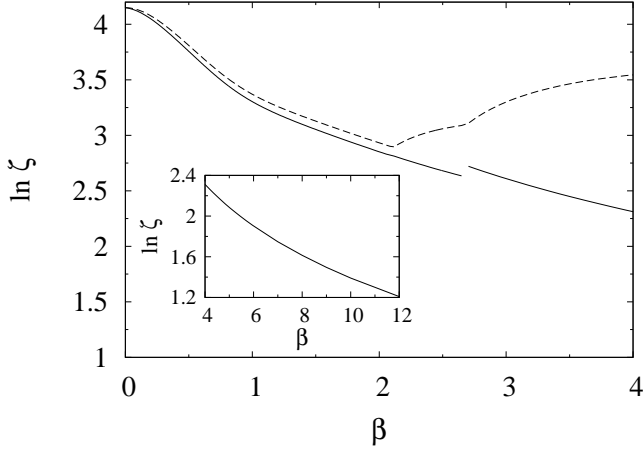
FIG. 12: $\ln\zeta$ vs. β in FTHFB for ^{148}Sm. Lines are as in Fig. 5.
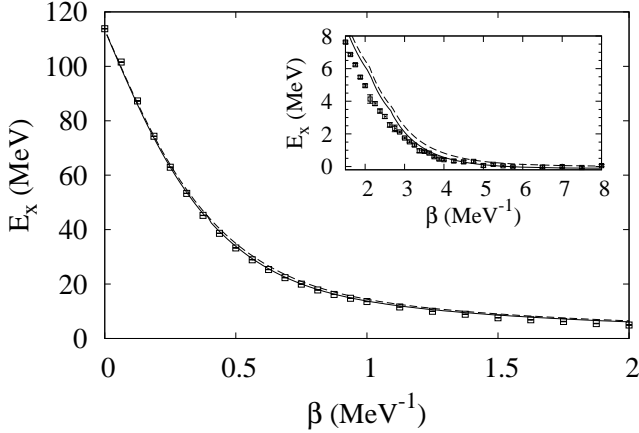
1. Excitation energies

FIG. 13: Excitation energy of ^{148}Sm as a function of inverse temperature β for $0 < \beta < 2$ MeV^{-1}, comparing the grand canonical HFB energy in Eq. (44) (dashed line) with the approximate canonical energy in Eq. (19) (solid line) and the SMMC results (open squares). The inset shows an expanded energy scale.

The ^{148}Sm thermal excitation energy function E_x vs. β in FTHFB is compared with the SMMC results in Fig. 13. The HFB energy is shown by the dashed line. The excitation energies at $\beta = 0$ are nearly equal, differing only by the missing correlation energy. The two kinks in the HFB curve, visible in the inset, are associated with the neutron and proton pairing phase transitions. The HFB excitation energy is higher than that of the SMMC, as to be expected from the higher limiting entropy of the grand canonical ensemble. We next calculate the approximate canonical projection of the HFB energy using Eq. (21). The result is closer to the SMMC for high β, We note that for $\beta < 2$ MeV^{-1}(i.e., for temperatures above the pairing transitions) , the absolute HF and HFB energies coincide, so that the HF excitation energy is lower than the HFB excitation energy by exactly the amount of pairing correlation energy in the ground state.

2. Entropies

The grand canonical HFB entropy (dashed line) and SMMC entropy (open squares) functions in ^{148}Sm are shown in Fig. 14 vs. β. Their absolute values are set by integrating from the $\beta = 0$ point, where their respective values are given in Table I. Both entropy functions approaches zero at large β, confirming the sum rule (6). The neutron and proton pairing transitions are also visible as kinks in the HFB entropy curve [26].
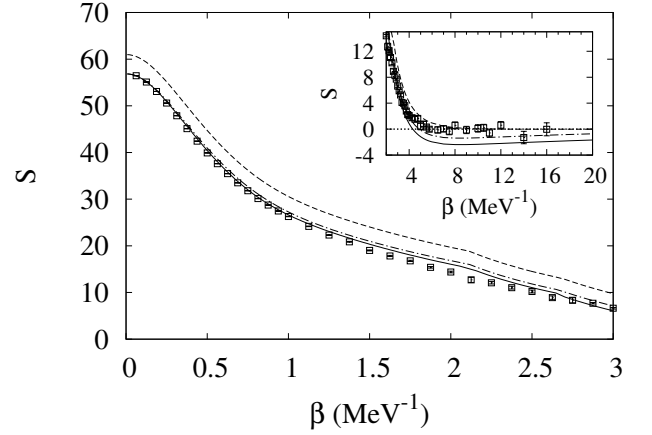

FIG. 14: Entropy functions of ^{148}Sm: the grand canonical HFB entropy (dashed line) and the approximate canonical HFB entropy in Eq. (20) with ζ given by Eq. (21) (solid line) are compared with the SMMC entropy (open squares). The dashed-dotted line is the entropy associated with the 3-D saddle-point point approximation, i.e., omitting the $\beta\delta E$ term in Eq. (20). The inset shows an expanded entropy scale at large β values.

We also show in Fig. 14 the approximate canonical HFB entropy in Eq. (20) where ζ is given by Eq. (21) in the discrete Gaussian model. Since the particle-number fluctuations in FTHFB remain relatively large even at low temperatures, similar results for ζ are found in the saddle-point approximation Eq. (16).

This approximate canonical entropy coincides with the SMMC at low values of β and overestimates the SMMC entropy around $\beta \sim 2$ MeV^{-1} , i.e., in the vicinity of the proton pairing transition. At larger values of β, for which a nonzero pairing condensate exists, the approxi-

mate canonical entropy is in overall agreement with the SMMC entropy up to $\beta \sim 3.5$ MeV^{-1} but at lower temperatures it becomes negative with a value of about -2 at $\beta \sim 7$ MeV^{-1} when the system reaches its HFB ground state. We note that if ζ were to be calculated using the HFB particle-number fluctuations (Eq. (47) in Eq. (25)), the large-β entropy would have been even more negative at ~ -4 units. A negative entropy at zero temperature is unphysical since there is only one state in the ensemble at zero temperature and the entropy should be zero. The HFB ground state violates particle-number conservation; the probability ζ^{-1} of having the proper proton and neutron numbers for ^{148}Sm at $\beta = 7$ MeV^{-1} is only ~ 0.17, hence the unphysical negative entropy at low temperatures.

To summarize the results of this section, we have not found a simple acceptable procedure to project the HFB onto a canonical ensemble if we require the correct entropy at high temperature and an error of less that one unit at low temperatures. We will comment further on this situation in the conclusion.

3. Angular momentum fluctuations

Eq. (39) which describes the angular momentum fluctuations in the FTHF approximation, has an additional contribution in FTHFB from a contraction in Wick's theorem that involves the anomalous density κ

$$\begin{aligned}\langle(\Delta J_q)^2\rangle &= \langle J_q^2\rangle - \langle J_q\rangle^2 \\ &= \mathrm{tr}[j_q(1-\varrho)j_q\,\varrho] - \mathrm{tr}[j_q\,\kappa j_q^*\,\kappa^*]\,. \quad (48)\end{aligned}$$

The additional contribution is negative, leading to a reduction in the mean-square moment of the angular momentum. This is just what one would expect as an effect of the pairing correlations.

In Fig. 15 we show the angular momentum fluctuations in ^{148}Sm as a function of β. The HFB solutions in ^{148}Sm is spherical at all temperatures so all directions are equal and we only need examine one of them. We compare $\langle J_z^2\rangle$ for HFB (solid line) with its SMMC (open squares) values. Below the pairing transition temperature, the HFB values are strongly suppressed compared to the spherical HF solution (dashed line), a known effect of pairing correlations. The SMMC values are further suppressed compared with HFB, in particular in the vicinity of the pairing transition. We observed substantial suppression also above the pairing transition temperature, indicating the persistence of pairing correlations in the SMMC results, even when the mean-field condensate no longer exists.

While the difficiency of the HFB around the phase transition is interesting to see, the magnitude of the error is not large enough to be of concern in calculating level densities.
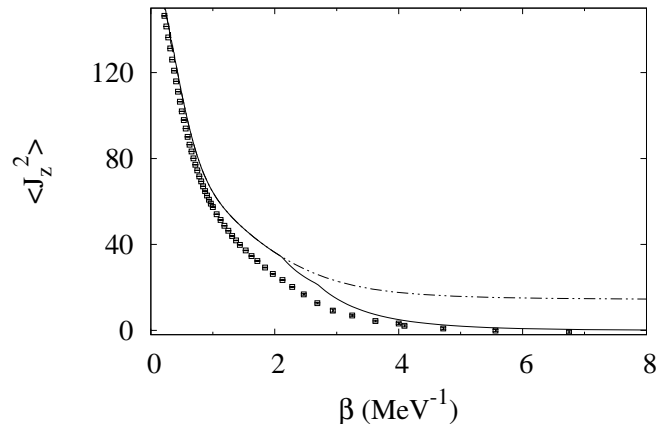

FIG. 15: Mean square angular momentum $\langle J_z^2\rangle$ in ^{148}Sm, comparing the HFB results (solid line) with the SMMC results (open squares). The dashed-double dotted line corresponds to the spherical HF solution.

4. State densities and level spacing

In Fig. 16 we show the HFB density of ^{148}Sm (solid line) in comparison with the SMMC state density (open squares). The HFB density was calculated with the canonical saddle-point approximation (4), taking the canonical entropy from Eq. (20) and ζ from Eq. (21). The result is practically indistinguishable when the δE term in Eq. (20) is omitted. We observe good agreement between the HFB and SMMC densities for excitation energies above the pairing transitions $E_x \geq 7$ MeV. At those energies, the HFB solution coincides with the HF solution, and the only role of the pairing is to reset the origin of the excitation energy scale by the pairing correlation energy. This good agreement may be fortuitous in view of two compensating errors in the HFB: the missing correlation energy in the ground state resets the excitation scale to lower the level density, while the many-body correlations increase the level density. This is seen as an increase in the effective mass of the quasi-particles [27]. Beyond that, for attractive interactions, the RPA correlation energy further raises the level density [28]. Nevertheless, we can take the present agreement as support for a popular model of the level density, namely the back-shifted Fermi gas. That model assumes that pairing correlations only affect the origin of the excitation energy scale.

At the same time, the calculated HFB level density is too small at low excitation energies. As with the calculated canonical entropy coming out negative, the problem relates to the violation of particle-number conservation in HFB.

Lastly we compute the neutron resonance spacing at threshold. For that we need the spin dependence of the level density. We use Eqs. (29) and (27), as was done
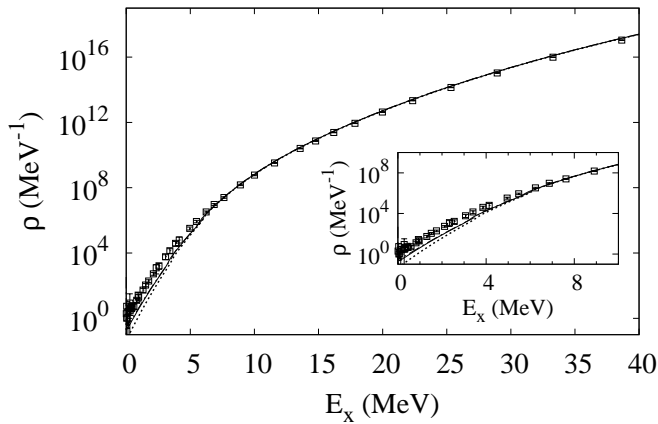
FIG. 16: State densities in ^{148}Sm. The HFB density (solid line) calculated from Eqs. (4), (20) and (21) is compared with the SMMC state density (open squares). The dotted line is the HFB density with ζ calculated from the particle-number fluctuations, Eq. (25). The inset is an expanded scale at low excitation energies.

for the SMMC, except that now $\rho(E)$ is taken to be the HFB density. This is justified since the HFB solution is spherical. The spin cutoff factor σ is taken from the HFB variance of J_z (see Fig. 15). As discussed previously, these fluctuations are larger in the HFB than in SMMC. However, this differences will affect the level density by less than a factor of two. We find in HFB a neutron resonance spacing at the neutron threshold of 4.1 eV, in very good agreement with the SMMC value of 3.7 eV (see Table III).

VI. CONCLUSION AND OUTLOOK

Our benchmarking of the finite-temperature HF and HFB approximations for level densities in heavy nuclei provides a quantitative assessment of the limitations of these mean-field theories. It also justifies their use under fairly broad sets of conditions. We have emphasized the relation between the grand canonical and canonical statistics because the mean-field theories are formulated in the grand canonical ensemble while the actual level densities are canonical. We first summarize our findings in Sec. VI A, then briefly survey the literature on the mean-field methods in use in Sec. VI B, and finally offer some remarks on a promising direction for improvement in Sec. VI C.

A. Findings

1. An important finding that echoes early work [15] is that the state density can be accurately calculated

from the canonical entropy function by the saddle-point method (which approximates the inverse Laplace transform of the canonical partition function). We improve upon this by showing that in simple cases (e.g., the independent-particle model with equidistant single-particle levels) one can obtain accurate results also starting from the grand canonical entropy.

2. Absent any broken symmetry in the mean-field solution, the particle-projected FTHF approximation gives accurate entropies and state densities.

3. Again echoing previous studies [29, 30], the phase transitions found in mean-field theory are washed out.

4. The pairing condensate phase in HFB is quite problematic because of the inherent violation of particle-number conservation. Nevertheless, level densities of strongly paired nuclei can be often calculated reliably at the neutron separation energy because the pairing condensate is no longer present at this energy, provided one can determine a reliable ground-state energy (which is affected by pairing correlations). This justifies the use of the back-shift approximation in simplified empirical theories [1, 31–33].

5. The spherical-to-deformed phase transition is problematic for a different reason. The ground state of a deformed nucleus has a continuous degeneracy in an unrestricted HF approximation. On the other hand, restricting the HF to axially symmetric fields gives a state density that is too low at low excitation energies. These states can be interpreted as intrinsic states on top of which of rotational bands are built. However, when the state density is estimated by a simple approximation of rotational bands built on top of intrinsic mean-field states, the resulting neutron resonance spacing at the neutron separation energy is too small (by about a factor of 4 in ^{162}Dy).

6. The frozen-potential (FP) approximation to FTHF is good for well-deformed nuclei up to the neutron separation energy (which is well below the shape transition excitation energy for a strongly deformed nucleus).

B. Implications

The current state-of-the-art methods for calculating level densities may be identified in the methods used in the RIPL compilation [34, 35]. Most of these methods are essentially phenomenological [36], but the HF is also used in the FP approximation. From our findings, that approximation is quite reasonable and easily compensated for by parameter adjustment. The RIPL compilation makes a strong distinction between the statistical and combinatorial methods. According to our finding 1 in Sec. VI A, these two methods should give almost identical results in the FP approximation. In fact, this was already seen in Ref. [2]. However, the contribution of the pairing condensate is included in the combinatorial method by a simple modification of the single-particle spectrum, which may not accurately reflect the many-

body nature of the condensate. Another combinatorial method was recently proposed in Ref. [24]. While this method treats the pairing condensate self-consistently, it is unclear how the reduction from the grand canonical to the canonical ensemble is carried out.

The calculations based on the FP approximation often include a phenomenological enhancement factor attributed to vibrational collective degrees of freedom. Such an enhancement is well-founded as an extension of mean-field theory to include small-amplitude quantal fluctuations of the fields around the mean-field solution [7]. However, in the early literature this effect was found to be rather small [28], and for the Hamiltonian employed here, we find no compelling need for it.

In view of our comparative benchmarking of a deformed and of a spherical nucleus, it would be interesting to revisit the arguments presented by Bjornholm, Bohr and Mottelson regarding the effects of rotational-symmetry breaking on the level density [23]. There is only a small difference between the experimental level densities or the benchmark level densities of the two nuclei we examined, ^{162}Dy and ^{148}Sm. In fact, we followed for ^{162}Dy the prescription described in Eqs. (8-10) of Ref. 23 for extracting the level densities from the band-head densities, and obtained a level density that is too high. Also, the benchmark entropies of both ^{162}Dy and ^{148}Sm are very similar for values of β in the range $\sim 1.5 - 3$ MeV^{-1}. We conclude that, except for the lowest excitation energies, deformation is less important than commonly assumed.

C. Outlook

It is clear that serious problems arise in the self-consistent mean-field theory and that some extension of the theory is needed if it is used to calculate level densities in the presence of mean-field condensates that are associated with symmetry breaking. In a deformed nucleus it is necessary to take into account an enhancement due to rotational bands, and in a nucleus with a strong pairing condensate we found no simple way to project from the grand canonical to the canonical ensemble. One desirable goal is a computational framework that applies equally well to spherical and to deformed nuclei, as well as those in between. The static path approximation (SPA) with the inclusion of number-parity projection (to capture pairing effects) satisfies this condition. The SPA was studied in the context of schematic Hamiltonians with promising results [30, 37]. One difficulty that has to be addressed is how to obtain an accurate ground-state energy, necessary to set the excitation energy scale for the level density.

The random-phase approximation (RPA) provides a powerful method to treat correlation energies beyond the mean-field approximation, even in the presence of degeneracies that are associated with the broken symmetries. With some exceptions [8, 38], the RPA has

mostly been applied in the framework of the SPA. In early studies it was found that the ground-state energy obtained in the SPA was not accurate enough to be useful for setting the excitation energy scale for the level densities. However, later model studies that included the RPA corrections to pairing have been quite successful [21, 37] and the method has been applied to physical systems [22]. We note also that the SPA+RPA with the inclusion of number-parity projection describes well thermodynamic properties of superconducting nanoscale metallic grains [39]. In the nuclear context it would be interesting to carry out a systematic study of the accuracy of the SPA and of the SPA+RPA for shell model Hamiltonians such as the ones used in the SMMC.

A different approach to nuclear level densities is the moment method, also known as the statistical spectroscopy approach. It requires the calculation of at least the first and second moments of the Hamiltonian, and so far it has been applied up to mid-mass nuclei [40, 41]. Recent progress in our understanding of the four lowest moments of the Hamiltonian were reported in Ref. [42], However, as with the SPA, accurate ground-state energies are needed to set the scale of excitation energies. It might also be interesting to carry out a comparative study similar to what we have done here for the mean-field approaches.

VII.   ACKNOWLEDGMENTS

Appendix I: accuracy of the saddle-point approximation

Here we use a simple model to assess the accuracy of the saddle-point approximations for the state density in Sec. II A and the approximate particle-number projections in Secs. II C and II D for the entropy. The model describes independent fermions populating equidistant energy levels. The only parameter in the model (in the limit when the number of single-particle levels is large) is the spacing of the single-particle states δ. The Hamiltonian of this system is

$$H = \delta \sum_{i=0}^{D-1}(i+1/2)a_i^\dagger a_i \qquad (49)$$

where δ is the single-particle level spacing and D is the total number of single-particle levels.

We first show that the factorization (26) of the grand canonical partition function is essentially exact in this model when T/δ, the temperature in units of the single-particle mean-level spacing, is much smaller than both the number of particles N and $D - N$. The key observation is that under these conditions the canonical partition function $Z_c(\beta)$, calculated with respect to the ground-state energy of the N particles (i.e., in terms of excitation energy) is *independent* of N. Changing N shifts the Fermi energy but since the single-particle spectrum is invariant under such a shift, the particle-hole excitations remain unchanged. A typical particle-hole excitation energy is of order T so the number of excited particles is typically smaller than N (under the above conditions).

The canonical partition function of a system with ground-state energy E_0 is given by $e^{-\beta E_0}Z_c(\beta)$ where $Z_c(\beta)$ is the partition calculated using the excitation energies. The N particle ground-state energy of the Hamiltonian (49) is given by $E_0 = N^2\delta/2$, and thus the N particle canonical partition is

$$Z_c(\beta, N) = e^{-\frac{1}{2}\beta N^2 \delta}Z_c(\beta) . \qquad (50)$$

We expand the grand canonical partition function $Z_{gc}(\beta, \alpha)$ for a value $\alpha = \alpha_0$ that gives an average number of particles N_0

$$\alpha_0 = \beta N_0 \delta , \qquad (51)$$

and use Eq. (50) to find

$$Z_{gc}(\beta, \alpha_0) \approx \sum_N e^{\alpha_0 N - \frac{1}{2}\beta N^2 \delta}Z_c(\beta) . \qquad (52)$$

The quasi-equality "$\approx$" is a reminder that the formula is valid for $T/\delta \ll N, D - N$. Using (51) we have

$$Z_{gc}(\beta, \alpha_0) \approx \sum_N e^{-\beta \frac{(N-N_0)^2}{2}\delta}e^{\frac{1}{2}\beta N_0^2 \delta}Z_c(\beta) . \qquad (53)$$

With the help of Eq. (50) for $N = N_0$, we can rewrite the last relation in the form

$$Z_{gc}(\beta, \alpha_0)e^{-\alpha_0 N_0} = Z_c(\beta, N_0)\left(\sum_N e^{-\beta \frac{(N-N_0)^2}{2}\delta}\right) \qquad (54)$$

This relation describes the factorization (26) of the grand canonical partition. The quantity in parenthesis is the partition function ζ of the discrete Gaussian model [see Eq. (25)], provided that the particle-number variance is $(\beta\delta)^{-1}$. Indeed

$$\langle(\Delta N)^2\rangle = \sum_{m=0}^{D} f_m(1 - f_m)$$

$$\approx \int_0^D dm \frac{e^{\beta m \delta - \alpha}}{(e^{\beta m \delta - \alpha} + 1)^2} = \frac{1}{\beta\delta} , \qquad (55)$$

where we have used $\beta N_0 \delta \gg 1$ and $\beta(D - N_0)\delta \gg 1$.

It is instructive to see how the particle-number projection works with a numerical example. We take the ensemble is a finite space, $(D, N) = (40, 20)$, chosen to have dimensions comparable to those we dealt with in the text.

The exact canonical entropy $S_c(\beta)$ (obtained by using exact particle-number projection) is shown in Fig. 17 by the solid line. It starts at $S(0) = \ln \binom{40}{20} = 25.65$ and approaches zero at large β.

We next turn to the grand canonical ensemble, in which we fix the chemical potential at each value of β to get the desired particle number in the ensemble average. The grand canonical entropy for the $(40, 20)$ model is shown as the dashed curve in Fig. 17. Here the starting entropy from Eq. (9) is 27.73, larger than the canonical entropy by 2.08 units. The approximate reduction to the canonical ensemble is carried out by Eq. (20). The result is shown as the dot-dashed curve in Fig. 17. It is accurate to within 0.1 of a unit over entire range of β. We also show for comparison the entropy calculated with Eq. (20) without the δE correction (dotted line). It is much less accurate, differing from the exact value by more than a half-unit for $\beta\delta > 1$.
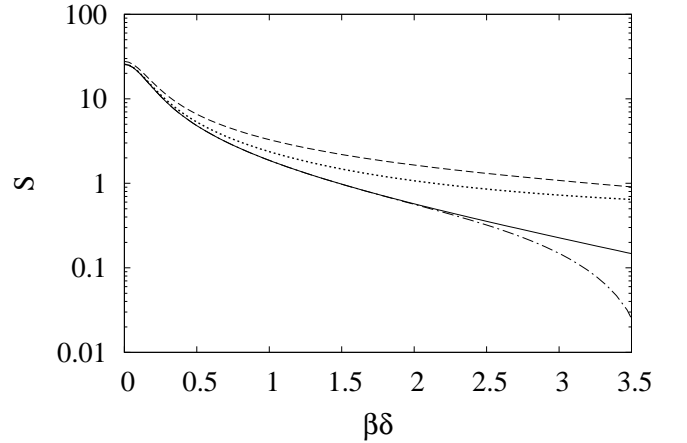

FIG. 17: Entropy of the $(D, N) = (40, 20)$ model as a function of β. See text for explanation.

The entropies of Fig. 17 are replotted in Fig. 18 as a function of excitation energy (in units of δ) E_x/δ. The entropy shown by the dashed line is the approximate canonical entropy of Eq. (20) which includes the contribution from δE; that contribution is omitted in the

entropy shown as the dotted line. The two are very close except at low excitation energies (see inset). The difference of the approximate canonical entropy from the true canonical entropy (solid line) can hardly be seen in the figure.
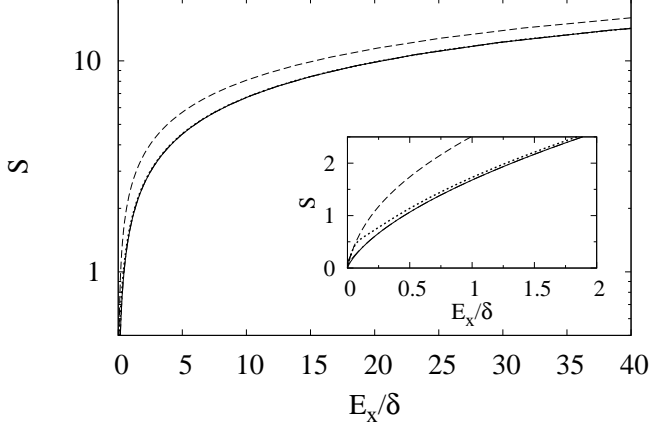

FIG. 18: Entropy of the $(D, N) = (40, 20)$ model as a function of excitation energy E_x/δ. See text for explanation.
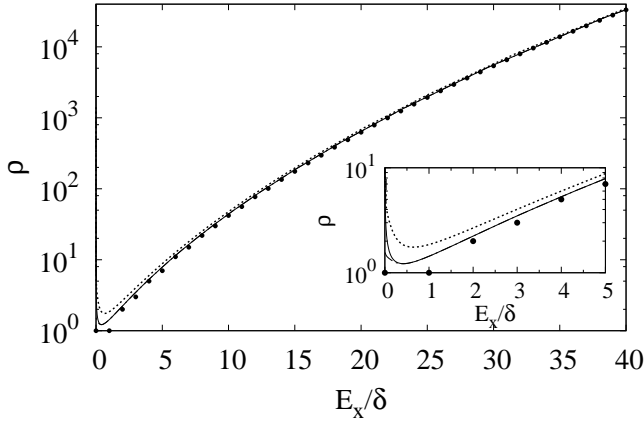

FIG. 19: State density for the Hamiltonian (49) with $(D, N) = (40, 20)$. See text for explanation.

We next turn to the state density itself. The excitation energy spectrum is $n\delta$ ($n = 0, 1, 2, \ldots$), and the state density for N particles is given by

$$\rho_N(E_x) = \sum_{n=0} \delta(E_x - n\delta) \, a(n) \qquad (56)$$

for $n < \min(N, D - N)$. Here $a(n) = 1, 1, 2, 3, 5, 7, 11, \ldots$ is the well-known partition of the integer n [43, 44]. The saddle-point approximation for the state density is also

well-known [44] and it has been shown to be accurate enough for our purposes for $n > 2$ [15].

Fig. 19 shows as solid circles the state density as the number of states within energy bins of width δ (i.e., the numbers $a(n)$). The ground state and first excited state are unique, and then there is an increasing density up to half the maximal energy. For comparison we also show by solid line the level density calculated from (4) using the canonical energy and entropy obtained by exact particle-number projection.

The state density in the standard saddle-point approximation is shown by the dotted line, while the state density of Eq. (4), in which the saddle-point prefactor is calculated from $dE_\zeta/d\beta$ (see Eq. (19)) gives the dashed-dotted line. This curve is hardly distinguishable from the solid line and improves the agreement with the exact result at low excitation energies. We observe that the improved saddle-point expression (20) and (19) is accurate to better than 10% to energies as low as 2δ. Since the low-lying region of the spectrum would be calculated by explicit methods anyway, we conclude that the improved saddle-point approximation is entirely adequate for statistical purposes.

Appendix II: thermodynamical consistency of the HF and HFB approximations

The key consistency condition of a finite-temperature theory in the grand canonical ensemble is the relation between S_{gc} and E_{gc} given by the equation analogous to Eq. (2) for the canonical ensemble. It can be easily derived from the relations (14) satisfied by the first logarithmic derivatives of $Z_{gc} = \text{Tr} \exp(-\beta\hat{H} + \alpha\hat{N})$. However, these derivatives are more subtle in the case of a mean-field Hamiltonian because the effective Hamiltonian in the density operator depends on the temperature and chemical potentials.

Here we prove that similar relations Eqs. (36) are indeed valid in the FTHF approximation. The proof follows from the fact that the theory is derived from the variational principle for the grand potential Ω [5, 6]. We write expression for the HF grand potential Ω_{HF} in the form

$$-\ln Z_{HF} = \beta\Omega_{HF} = \beta E_{HF} - S_{HF} - \alpha N_{HF} . \qquad (57)$$

where E_{HF}, S_{HF} were defined in Eqs. (33) and (34).

The derivative of Eq. (57) with respect to β has a contribution E_{HF} from the explicit dependence on β. However, there is in principle also a contribution from the implicit dependence on β in E_{HF}, S_{HF} and N_{HF}. To see that they vanish we go back to the many-body uncorrelated density matrix $\hat{D}_{HF}$ that was the trial density of the variational principle. Taking that as the fundamental

variable, the relevant derivative is

$$-\frac{\partial \ln Z_{HF}}{\partial \beta}\Big|_\alpha = \frac{\partial(\beta\Omega_{HF})}{\partial\beta}\Big|_\alpha$$

$$= E_{HF} + \frac{\delta(\beta\Omega_{HF})}{\delta\hat{D}_{HF}}\Big|_{\beta,\alpha}\frac{\partial\hat{D}_{HF}}{\partial\beta} . \quad (58)$$

Since $\hat{D}_{HF}$ is a variational solution at fixed β and α, it follows that

$$\frac{\delta(\beta\Omega_{HF})}{\delta\hat{D}_{HF}}\Big|_{\beta,\alpha} = 0 , \qquad (59)$$

and the second contribution on the right-hand side of Eq. (58) vanishes. The thermodynamic consistency of the finite-temperature HFB can be proven in the same way.

[1] D. Gambacurta, D. Lacroix, and N. Sandulescu, Phys. Rev. C **88**, 034324 (2013).

[2] S. Hilaire and S. Goriely, Nucl. Phys. A **779**, 63 (2006).

[3] S. Goriely, S. Hilaire and A.J. Koning, Phys. Rev. C **78**, 064307 (2008).

[4] P. Demetriou and S. Goriely, Nucl. Phys. **A695** 95 (2001).

[5] A.L. Goodman, Nucl. Phys. **A352** 30 (1981).

[6] K. Tanabe, K. Sugawara-Tanabe and H.J. Mang, Nucl. Phys. **A357** 20 (1981).

[7] A.K. Kerman and S. Levit, Phys. Rev. C **24**, 1029 (1981); A.K. Kermin, S Levit and T. Troudet, Ann. Phys. **148** 436 (1983).

[8] D. Vautherin and N. Vinh Mau, Phys. Lett. B **120**, 261 (1983); N. Vinh Mau and D. Vautherin, Nucl. Phys. A **445**, 245 (1985).

[9] G.H. Lang, C.W. Johnson, S.E. Koonin, and W.E. Ormand, Phys. Rev. C **48**, 1518 (1993).

[10] Y. Alhassid, D.J. Dean, S.E. Koonin, G.H. Lang, and W.E. Ormand, Phys. Rev. Lett. **72**, 613 (1994).

[11] H. Nakada and Y. Alhassid, Phys. Rev. Lett. **79**, 2939 (1997).

[12] Y. Alhassid, S. Liu and H. Nakada, Phys. Rev. Lett. **83**, 4265 (1999).

[13] A. Bohr and B. Mottelson, *Nuclear Structure*, Vol. I, (Benjamin, 1975).

[14] The equivalence follows directly from the identity for symmetric matrices A: $\det A = \det B(a_{11} - \vec{a}_1 \cdot B^{-1} \cdot \vec{a}_1)$, where a_{11} is the element of A in the first row and column, B is the minor obtained from A by striking out the first row and column, and $\vec{a}_1|_i = a_{1,i+1}$.

[15] T. Ericson, Advances in Physics **6**, 425 (1960).

[16] Small bad-sign interaction terms can be treated using the extrapolation method of Ref. [10].

[17] W.E. Ormand, D.J. Dean, C.W. Johnson, et al., Phys. Rev. C **49**, 1422 (1994).

[18] Y. Alhassid, L. Fang and H. Nakada, Phys. Rev. Lett. **101**, 082501 (2008).

[19] C. Özen, Y. Alhassid, and H. Nakada, Phys. Rev. Lett. **110**, 042502 (2013).

[20] C. Esebbag and J.L. Egido, Nucl. Phys. A **552**, 205 (1993).

[21] R. Rossignoli, N. Canosa, and P. Ring, Phys. Rev. Lett. **80**, 1853 (1998).

[22] K. Kaneko, M. Hasegawa, et al., Phys. Rev. C **74**, 024325 (2006); K. Kaneko and A. Schiller, Phys. Rev. C **76**, 064306 (2007).

[23] S. Bjørnholm, A. Bohr and B.R. Mottelson, *Physics and Chemistry of Fission 1973* (IAEA, Austria, 1974), p. 367.

[24] H. Uhrenholt, S. Åberg, A. Bobrowolski, et al., Nucl. Phys. A **913**, 127 (2013).

[25] G.F. Bertsch and L.M. Robledo, Comp. Phys. Comm. **185**, 3406 (2014).

[26] The mean-field phase transition can be seen even more clearly as a discontinuity in the heat capacity $C = \beta dS/d\beta$.

[27] V. M. Galitskii, Sov. Phys. JETP **34**, 151 (1958).

[28] D. Vautherin, Adv. Nucl. Phys. **22**, 123 (1996).

[29] A.L. Goodman, Phys. Rev. C **29** 1887 (1984).

[30] R. Rossignoli, et al., Nucl. Phys. **A605** 1 (1996).

[31] T. Rauscher, F.-K. Thielemann, and K.-L. Kratz, Phys. Rev. C **56**, 1613 (1997).

[32] T. von Egidy and D. Bucurescu, Phys. Rev. C **72**, 044311 (2005).

[33] I. Poitoratska, et al., Phys. Rev. C **89**, 054322 (2014).

[34] The RIPL3 database containing tables of experimental level densities can be accessed at https://www-nds.iaea.org/RIPL-3/resonances/.

[35] R. Capote, et al., Nucl. Data Sheets bf 110, 3107 (2009).

[36] A.J.Koning, S. Hilaire and S. Goriely, Nucl. Phys. A **810**, 13 (2008).

[37] G. Puddu, P.F. Bortignon, and R.A. Broglia, Ann. Phys. (NY) **206**, 409 (1991).

[38] N. Quang Hung and N. Dinh Dang, Phys. Rev. C **81**, 057302 (2010).

[39] K.N. Nesterov and Y. Alhassid, Phys. Rev. B **87**, 014515 (2013), and references therein.

[40] R.A. Sen'kov and M. Horoi, Phys. Rev. C 82, 024304 (2010).

[41] R.A. Sen'kov, M. Horoi, and V.G. Zelevinsky, Phys. Lett. B **702**, 413 (2011).

[42] E. Teran and C.W. Johnson, Phys. Rev. C **73**, 024303 (2016).

[43] L. Euler (1753), cited by Ericson [15].

[44] M. Abramowitz and I. Stegun, *Handbook of Mathematical Functions* (National Bureau of Standards, 1964), Sec. 24.2.1.